Journal of Energy Storage 72 (2023) 108649

Contents lists available at ScienceDirect

Journal of Energy Storage

journal homepage: www.elsevier.com/locate/est

Research papers

A fractional-order electrochemical lithium-ion batteries model considering electrolyte polarization and aging mechanism for state of health estimation ☆

Guorong Zhu [a], Chun Kong [a], Jing V. Wang [a], Jianqiang Kang [b,c,*], Qian Wang [a], Chunhu Qian [d]

[a] School of Automation, Wuhan University of Technology, Wuhan 430070, PR China
[b] Hubei Key Laboratory of Advanced Technology for Automotive Components, Wuhan University of Technology, Wuhan 430070, PR China
[c] Hubei Collaborative Innovation Center for Automotive Components Technology, Wuhan 430070, PR China
[d] Flextech Company, Wuhan 430070, PR China

ARTICLE INFO

Keywords:
Lithium-ion batteries
Simplified electrochemical model
SEI layer
Lithium plating
State of health estimation

ABSTRACT

Accurate state of health (SOH) estimation of lithium-ion batteries is critical for the safe and reliable operation of battery power system. To achieve better SOH estimation with low computational complexity, a fractional-order model considering electrolyte polarization and aging mechanism (FOMeA) is proposed. The proposed model simplifies solid phase lithium-ion distribution with fractional-order Padé approximation and electrolyte phase lithium-ion distribution with a two-state system. The solid electrolyte interphase (SEI) layer formation and lithium plating side reactions, which lead to battery aging, are modeled to establish the relationship between the cycle number and the aging parameters in the proposed simplified electrochemical model. Finally, FOMeA is compared with the pseudo-2D (P2D) aging model. The result shows that FOMeA can achieve accurate voltage prediction and SOH estimation in whole battery cycle life, and greatly save computational time.

1. Introduction

Lithium-ion batteries have been widely used as a power source in smart phones, electrical vehicles, and other energy storage devices due to their long cycle life, high charge and discharge efficiency, and high energy density [1]. Lithium-ion batteries have a longer cycle life compared with other batteries. Lithium-ion batteries still retain 80% depth of discharge even after being cycled for 1000 times [2]. However, the lifetime of electrical vehicles' life-time is designed to be more than 10 years, and energy storage devices also require frequent charging and discharging [3]. The lifetime of lithium-ion batteries is difficult to completely cover the lifespan of electrical vehicles and energy storage devices. As lithium-ion batteries age, their capacity decreases, internal resistances increase, and charge and discharge performance decreases because of various types of polarization within the batteries. Aged batteries are not qualified for high rate charging and discharging [4]. The charge and discharge efficiency of aged batteries decreases because of the increase in their resistance. Aged batteries also produce more heat, accelerating the temperature rise of the batteries, especially during high rate charging and discharging. Furthermore, aged batteries are more likely to experience thermal runaway, which threatens the safety of people's lives and property [5]. Therefore, accurate estimation of the state of health (SOH) of batteries is crucial.

Lithium-ion batteries are subject to two main side reactions that contribute to their degradation. One is the solid electrolyte interphase (SEI) layer formation, which mainly occurs at the interface between negative solid phase particles and the electrolyte of negative electrode [6]. Recyclable lithium ions react with the electrolyte to form an SEI film that covers the surface of negative electrode particles. The growing SEI layer leads to a decrease in the effective surface area of the electrode and ionic conductivity [7]. Phul et al. [8] developed a mathematical model to study the potential drop across the SEI layer and the capacity fading of lithium-ion batteries. They found that capacity fade is dependent on the kinetics of the reaction as compared to diffusion. Wang et al. [9] reviewed the revolutionary SEI layer modeling on the negative electrode and compared these models with experiments. Another degradation side reaction is the lithium plating, which also occurs on the surface of negative electrode particles [10]. When the lithium-ion flux in the SEI layer is large and the lithium-ion diffusion in the negative electrode is slow, lithium plating is more likely to occur [11]. Ren et al. [12] proposed an electrochemical model that incorporates lithium plating and stripping reactions. This model successfully predicts the characteristic voltage plateau during the rest period after high rate charging at low temperatures. Yang et al. [13] found that uneven electrolyte distribution can induce uneven lithium

☆ This is the results of the research project.

* Corresponding author at: Hubei Key Laboratory of Advanced Technology for Automotive Components, Wuhan University of Technology, Wuhan 430070, PR China.
E-mail address: kjqiang@whut.edu.cn (J. Kang).

https://doi.org/10.1016/j.est.2023.108649
Received 13 April 2023; Received in revised form 16 July 2023; Accepted 7 August 2023

plating behavior and that saturated lithium-graphite compounds with sufficient electrolyte are favorable to plating lithium. The SEI layer formation and lithium plating side reactions lead to the loss of lithium ions, increase in internal resistance, and damage to charge and discharge performance of the battery [14,15]. Tian et al. [16] analyzed the degradation state of lithium-ion batteries in macroview. The author constructed a fractional-order model and identified its parameters, and also, they analyzed the battery aging mechanism based on the identified open-circuit voltage by the means of an incremental capacity analysis method.

When the maximum available capacity of the cell reaches 80% of its nominal capacity, it is considered to have reached the end of its life [17]. Fully charging and discharging a cell with a constant current rate are necessary to measure its capacity. However, in practical usage, the cell is rarely fully charged and discharged with constant current rate. Thanks to the advanced machine learning models, the cell capacity estimation can be easily achieved by mapping the aging factors to the labeled cell capacity. The factors affecting battery aging, which contains applied current, cycle numbers, and temperature, can be precisely measured in laboratory. The precise cell capacity can be measured with 1C rate constant current charge and discharge in laboratory. Machine learning models capture the characteristics of input data, and learn the internal law of input data. Although training machine learning models are computational complex, it is fast to calculate the forward channels of machine learning models. Xiong et al. [18] proposed a convolutional neural network to perform cell capacity estimation by taking only raw impedance spectra as input, and they developed two large battery degradation datasets which contains over 4700 impedance spectra to validate the proposed model. Shen et al. [19] proposed a deep convolutional neural network with ensemble learning and transfer learning for capacity estimation of lithium-ion batteries. The proposed model was verified with a target dataset consisting of 20 commercial 18 650 lithium-ion cell, and compared with random forest regression and Gaussian process regression methods. Although advanced machine learning models have achieved good capacity estimation, they cannot explain the internal electrochemical mechanisms that degrade lithium-ion batteries, and cannot predict the internal state of lithium-ion batteries while the cell cycles. In many scenarios, there is no large dataset for the machine learning model to be trained, which may cause the machine learning model to be overfitted, resulting in weak generalization. The machine learning model is trained to achieve accurate predictions only for specific cells under specific dynamics.

Physics-based lithium-ion batteries model can accurately predict not only the battery capacity, but also the internal state of the battery while cycling. Doyle et al. [20] proposed a pseudo-2D (P2D) electrochemical model for lithium-ion batteries that accurately predicts the cell voltage and describes the cell inner physical mechanism. However, the P2D model has a series of strongly coupled nonlinear partial differential equations, which makes it challenging to calculate, and many parameters need to be identified in the model [21]. Hence, the P2D model is difficult to apply in a battery management system (BMS). A single particle (SP) model of lithium-ion batteries was proposed to reduce the computational complexity with the reduced number of model parameters [22]. The SP model treats the electrode as a single particle and ignores the electrolyte polarization, greatly simplifying P2D model's structure. However, an infinite-order transcendental transfer function is required to describe the diffusion of solid phase lithium-ions. Guo et al. [23] proposed a fractional-order model (FOM) based on the SP model, which further simplifies the solid phase diffusion with fractional-order Padé approximation. Although the SP model simplifies the P2D model, it cannot achieve high-accuracy voltage prediction with a high rate current charge and discharge due to ignoring the electrolyte polarization [24]. To improve the voltage prediction accuracy of the SP model at high rate current dynamics, polarization in electrolyte can be considered into the SP model. Moura et al. [25] presented an SP model with electrolyte dynamics (SPMe). The simulation results show that SPMe can still achieve high-accuracy voltage prediction, even under 5C rate constant current discharge. Li [26,27] et al. proposed a physics-based fractional-order model for state of energy estimation which considers electrolyte polarization with a first-order resistance-capacitor transfer function. With this model, the number of electrochemical parameters that needs identification was reduced from 30 to 9, making modeling more easily. However, the above electrochemical models did not consider the cell aging mechanism. What is more, they can predict voltage and capacity well with a new cell, but cannot fit the aged cell.

In this paper, a fractional-order model considering electrolyte polarization and aging mechanism (FOMeA) is proposed to apply the electrochemical lithium-ion batteries model in BMS and achieve better SOH estimation for the cell. The FOMeA considers SEI layer formation and lithium plating-stripping side reactions which affect the aging parameters in the fractional-order model considering electrolyte polarization (FOMe). The three original contributions of FOMeA are as follows:

(a) The FOM is developed by considering electrolyte polarization, which can achieve high-accuracy voltage and capacity prediction at high current rates with low computation complexity.
(b) The SEI layer formation side reaction model and the lithium plating-stripping side reaction model are established. The aging parameters affected by SEI layer growing and lithium plating in FOMe are analyzed.
(c) The relationship between aging parameters affected by aging mechanisms and the cycle number is established. The FOM considering electrolyte polarization with an aging mechanism is proposed, which can achieve accurate voltage prediction and SOH estimation during whole life time of the cell.

2. Aging mechanism model

Lithium-ion batteries age with the recycling of charge and discharge, causing the cell capacity to fade and resistance to increase. The SEI formation and the lithium plating-stripping are the two main side reactions which cause the cell ages.

2.1. Growth of SEI layer

The SEI layer primarily grows at the electrode–electrolyte interface on the negative electrode surface. Generally, the negative electrode active material is graphite, and the electrolyte solvent is ethylene carbonate (EC). The main compounds of the SEI layer formation side reaction products are Li_2CO_3 and $(CH_2OCO_2Li)_2$ [28]. The SEI layer formation side reaction equation can be described as Eqs. (1) and (2). The positive electrode material is assumed not to be involved in the SEI growing side reaction.

$$2Li^+ + 2e^- + EC \rightarrow C_2H_4 \uparrow + Li_2CO_3 \downarrow \quad (1)$$

$$2Li^+ + 2e^- + 2EC \rightarrow C_2H_4 \uparrow + (CH_2OCO_2Li)_2 \downarrow \quad (2)$$

As the cell ages, the SEI layer on the negative electrode surface grows, reducing the contact area between lithium-ion and the active electrode material and increasing the internal resistance. The reduction side reaction consumes lithium-ion, causing some electrode particles to become isolated with lithium-ion trapped inside by the side reaction products. This condition results in lithium-ion loss and active electrode material loss, leading to a decrease in the cell's power and capacity.

The SEI layer formation reaction is irreversible, and only the reduction reaction occurs, so it can be described by a Tafel equation [17], as shown in Eq. (3).

$$j_{SEI} = -a_s i_{0,SEI} \exp(-\frac{\alpha_{SEI} n_{SEI} F}{R_g T} \eta_{SEI}) \tag{3}$$

where j_{SEI} is the SEI layer formation reaction rate, $i_{0,SEI}$ is the reference exchange current density of the reaction, α_{SEI} is the transfer coefficient, n_{SEI} is the number of lithium-ion moles participated in the SEI layer formation reaction with a value of two, F is the Faraday constant, R_g is the molar gas constant, and T is the cell temperature. α_s is the specific surface area, which can be calculated as

$$a_s = 3\epsilon / R_s \tag{4}$$

where ϵ is the volume fraction of solid phase, and R_s is the radius of electrode particles. η_{SEI} is the SEI layer formation reaction overpotential, which is defined as

$$\eta_{SEI} = \varphi_s - \varphi_e - U_{SEI} - \frac{R_{SEI}}{a_s} j \tag{5}$$

where φ_s and φ_e are solid and electrolyte phase potentials, respectively. U_{SEI} is the equilibrium potential of the SEI formation reaction, which is set to be 0.4 V. R_{SEI} is the resistance of SEI layer. j is the total lithium-ion flux which takes part in electrochemical reactions.

2.2. Lithium plating-stripping

When a cell charges at low temperature with a high current rate, lithium plating-stripping may easily occur on the negative electrode surface [29]. Lithium plating-stripping is a reversible reaction that can be described by using the Butler–Volmer equation, as shown in Eq. (6)

$$j_{LP/S} = a_s i_{0,LP}(\exp(\frac{\alpha_{a,LS} F}{R_g T} \eta_{LP/S}) - \exp(-\frac{\alpha_{c,LP} F}{R_g T} \eta_{LP/S})) \tag{6}$$

where $i_{0,LP}$ is the reference exchange current density of the lithium plating-stripping side reaction, $\alpha_{a,LS}$ and $\alpha_{c,LP}$ are the anodic and cathodic charge transfer coefficients of the lithium plating-stripping reaction, respectively, and $\eta_{LP/S}$ is the overpotential of the reaction. When $\eta_{LP/S} < 0$, lithium plating occurs on the negative electrode surface. The lithium plating overpotential η_{LP} can be expressed as

$$\eta_{LP} = \min(0, \varphi_s - \varphi_e + U_{LP} - \frac{R_{SEI}}{a_s} j) \tag{7}$$

where U_{LP} is the overpotential of lithium plating-stripping, which is measured with respect to Li and is equal to 0 V. Some of the plated lithium will react with the electrolyte to form a secondary SEI layer on the plated lithium surface. During cell resting and discharging, some of the plated lithium will strip into the electrolyte if the lithium stripping overpotential η_{LS} exceeds 0 V. The lithium stripping overpotential η_{LS} can be expressed as

$$\eta_{LS} = \max(0, \varphi_s - \varphi_e + U_{LP} - \frac{R_{SEI}}{a_s} j) \tag{8}$$

The chemical equation for lithium plating-stripping can be described as Eqs. (9), (10).

$$\mathrm{Li^+ + e^-} \rightarrow z_1 \mathrm{Li}_{rev} \downarrow + z_2 \mathrm{Li}_{dead} \downarrow + z_3 SEI_{\mathrm{sec}} \tag{9}$$

$$\mathrm{Li}_{rev} \downarrow \rightarrow \mathrm{Li^+ + e^-} \tag{10}$$

where Li_{rev} represents the plated reversible lithium that can be stripped into the electrolyte during resting and discharging, Li_{dead} is the plated dead lithium that is isolated by the secondary SEI layer and cannot be stripped into the electrolyte, and SEI_{sec} is the secondary SEI layer generated by the reaction between the plated lithium and the electrolyte solvent, which covers on the surface of the plated dead lithium. z_1, z_2, and z_3 are the proportion of the three products generated by lithium plating-stripping reaction, respectively. The values of z_1, z_2, and z_3 are 0.775, 0.175, and 0.05, respectively, which are identified to fit the experimental data in [12].

3. Simplified electrochemical aging model for SOH estimation

3.1. Physics-based FOM considering electrolyte polarization

FOMe is a simplified electrochemical model of lithium-ion batteries, which assumes that the applied current is uniformly distributed over all electrode particles. Therefore, the positive and negative electrodes can be regarded as a single particle. Different from SP model, FOMe applies the fractional-order Padé approximation method to simplify lithium-ion diffusion in the solid phase, so that the surface lithium-ion concentration of electrodes can be easily calculated. FOMe considers the lithium-ion distribution in the electrolyte with a two-state system [30], which helps FOMe achieve accurate voltage prediction at a high current rate. The structure of FOMe is shown in Fig. 1.

In accordance with Fick's second law and solid phase lithium-ion diffusion boundary conditions, the relationship between the change in solid surface lithium-ion concentration after removing the integrator pole $\Delta\tilde{c}_{s,i}^{surf} = \tilde{c}_{s,i}^{surf} - c_{s,i}^{mean}$ and the applied current I can be expressed as

$$\frac{\Delta\tilde{c}_{s,i}^{surf}}{I} = \frac{\tau_i}{3\epsilon_{s,i} F A L_i} \left[\frac{1}{\sqrt{\tau_i s} \coth\left(\sqrt{\tau_i s}\right) - 1} - \frac{3}{\tau_i s} \right] \tag{11}$$

where $i = n, p$ represents the negative and positive electrode of the cell, respectively, I is the applied current (<0 on discharge), $\epsilon_{s,i}$ is the solid phase volume fraction, F is the Faraday constant, A is the area of electrodes, L_i is the length of electrodes, s is the complex frequency, and τ_i is the diffusion time constant, which is defined as

$$\tau_i = \frac{R_{s,i}^2}{D_{s,i}} \tag{12}$$

where $R_{s,i}$ is the particle radius of electrode particles, and $D_{s,i}$ is the solid phase diffusion coefficient.

Eq. (11) is a transcendental transfer function, and obtaining the rigorous solution of the transcendental transfer function is computationally complex. Hence, the fractional-order Padé approximation is applied to simplify Eq. (11). The simplified transfer function is shown as

$$\frac{\Delta\tilde{c}_{s,i}^{surf}}{I} = \frac{\tau_i}{3\epsilon_{s,i} F A L_i} \left[\frac{0.24419}{1 + 0.14257\sqrt{\tau_i s}} \right] \tag{13}$$

The solid phase stoichiometry of the electrode is defined as the ratio of the current lithium-ion concentration to the maximum lithium-ion concentration of electrodes. Therefore, the solid phase initial stoichiometry and the solid phase average stoichiometry can be expressed as

$$\theta_i^0 = \frac{c_{s,i}^0}{c_{s,i}^{\max}}, \quad \theta_i^{mean} = \frac{c_{s,i}^{mean}}{c_{s,i}^{\max}} \tag{14}$$

where $c_{s,i}^0$ is the initial lithium-ion concentration of electrodes, $c_{s,i}^{mean}$ is the average lithium-ion concentration of electrodes, and $c_{s,i}^{max}$ is the maximum lithium-ion concentration of electrodes. The relationship between θ_i^0 and θ_i^{mean} can be expressed as

$$\theta_n^{mean} = \theta_n^0 + \frac{1}{Q_n} \int_0^{t_k} I(t)dt, \; \theta_p^{mean} = \theta_p^0 - \frac{1}{Q_p} \int_0^{t_k} I(t)dt \tag{15}$$

where t_k is the total operation time. Q_p and Q_n are positive and negative electrode capacity, which can be calculated as

$$Q_i = A L_i F \epsilon_{s,i} c_{s,i}^{max}, \quad i = n, p \tag{16}$$

The solid phase surface stoichiometry of electrodes particles θ_i^{surf} can be calculated as

$$\theta_n^{surf} = \theta_n^{mean} + \frac{\Delta\tilde{c}_{s,n}^{surf}}{c_{s,n}^{\max}}, \; \theta_p^{surf} = \theta_p^{mean} - \frac{\Delta\tilde{c}_{s,p}^{surf}}{c_{s,p}^{\max}} \tag{17}$$

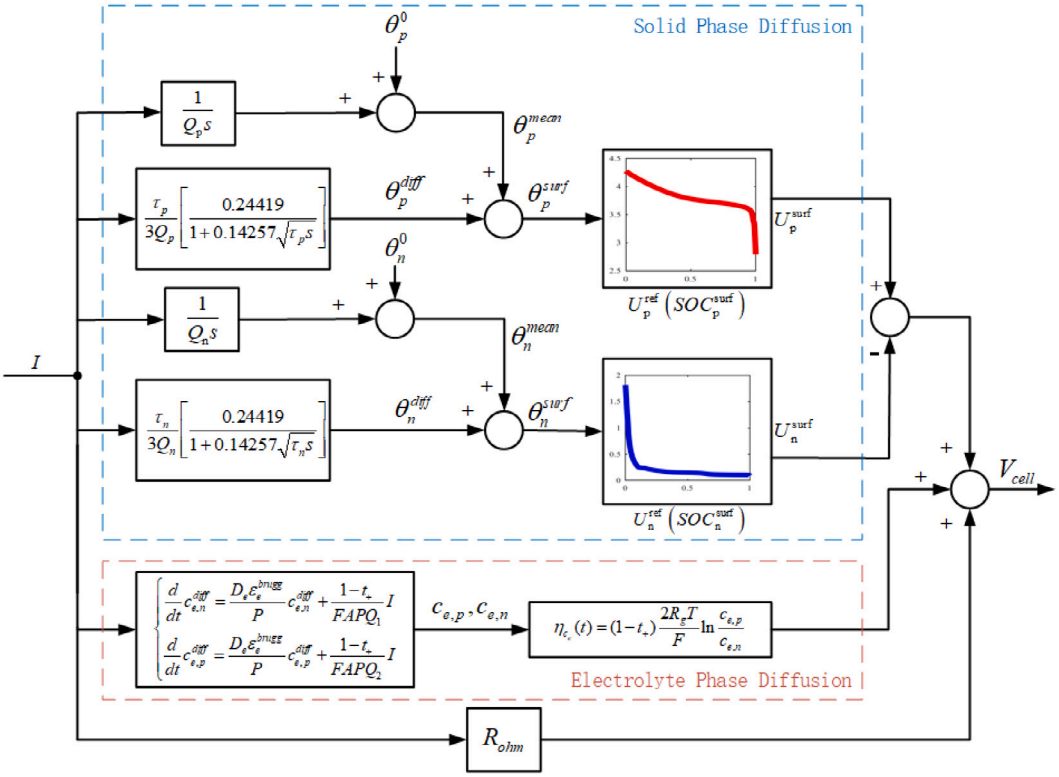

Fig. 1. The structure of FOMe.

The electrode potential is related to the solid phase surface stoichiometry of the electrode. The electromotive force E is defined as the difference between the positive electrode potential and negative electrode potential, as shown in Eq. (18)

$$E = U_p(\theta_p^{surf}) - U_n(\theta_n^{surf}) \tag{18}$$

where $U_i(\cdot)$ is the electrode potential as a function of the solid phase stoichiometry.

The electrolyte polarization overpotential is caused by the uneven distribution of electrolyte lithium-ion concentration on the electrode thickness direction [31]. For simplification, the electrolyte phase volume fractions of the positive electrode, separator, and negative electrode of the cell are assumed to be equal [32]. The change in the electrolyte phase lithium-ion concentration at the terminal of the positive and negative electrodes can be simplified as

$$\begin{cases} \frac{d}{dt}c_{e,n}^{diff} = \frac{D_e\varepsilon_e^{brugg}}{P}c_{e,n}^{diff} + \frac{1-t_+}{FAPQ_1}I \\ \frac{d}{dt}c_{e,p}^{diff} = \frac{D_e\varepsilon_e^{brugg}}{P}c_{e,p}^{diff} + \frac{1-t_+}{FAPQ_2}I \end{cases} \tag{19}$$

where $c_{e,i}^{diff} = c_{e,i} - c_e^0$ is the difference between the electrolyte phase lithium-ion concentration at electrode terminal $c_{e,i}$ and the initial electrolyte phase lithium-ion concentration c_e^0. D_e is the electrolyte phase diffusion coefficient, ε_e is the electrolyte phase volume fraction, $brugg$ is the Bruggman coefficient, and t_+ is the particle migration number. P, Q_1, and Q_2 can be calculated as

$$\begin{cases} P = -\varepsilon_e(\frac{1}{3}L_n^2 + L_n x_{equ} + \frac{1}{2}x_{equ}^2) \\ Q_1 = -\frac{2}{L_n + 2x_{equ}} \\ Q_2 = -\frac{2}{L_p + 2(L_{sep} - x_{equ})} \\ x_{equ} = \frac{-2L_n^2 + 3L_{sep}^2 + 2L_p^2 + 6L_{sep}L_p}{6(L_n + L_{sep} + L_p)} \end{cases} \tag{20}$$

where L_p, L_n, and L_{sep} are the thicknesses of positive electrode, negative electrode, and separator, respectively.

The concentration of lithium ions in the electrolyte phase at the terminals of the positive and negative electrodes directly affects the electrolyte polarization overpotential. The electrolyte polarization overpotential η_{c_e} can be calculated using Eq. (21) based on the concentration of lithium ions in the electrolyte phase at the terminals of the two electrodes.

$$\eta_{c_e}(t) = (1 - t_+)\frac{2R_gT}{F}\ln\frac{c_{e,p}}{c_{e,n}} \tag{21}$$

The activation polarization overpotential η_{ct} of the two electrodes can be calculated by using the Butler–Volmer kinetics equation, as shown in Eqs. (22) and (23).

$$\eta_{ct} = \frac{2R_gT}{F}\left[\ln(\sqrt{m_p^2 + 1} + m_p) - \ln(\sqrt{m_n^2 + 1} + m_n)\right] \tag{22}$$

$$m_i = 0.5j_i/[k_i(c_{e,i})^{0.5}(c_{s,i}^{\max} - c_{s,i}^{surf})^{0.5}(c_{s,i}^{surf})^{0.5}] \tag{23}$$

where k_i is the electrochemical reaction coefficient, j_i is the pole wall flux of lithium-ion intercalation into or deintercalation from the electrode particles, which can be calculated as

$$j_i = \frac{IR_{s,i}}{3\varepsilon_{s,i}FAL_i} \tag{24}$$

The ohmic resistance is a lumped parameter that describes the high-frequency dynamic response inside the cell. It is mainly composed of solid phase charge transfer resistance $R_{s,ohm}$, electrolyte phase charge transfer resistance $R_{e,ohm}$, SEI layer resistance R_{SEI}, lithium-ion plating resistance R_{Li}, and contact resistance R_{cont}. The ohmic resistance can be calculated as

$$R_{ohm} = R_{s,ohm} + R_{e,ohm} + R_{SEI} + R_{Li} + R_{cont}. \tag{25}$$

The terminal voltage of the cell is the sum of electromotive force, electrolyte polarization overpotential, electrochemical reaction overpotential, and ohmic resistance overpotential. The terminal voltage of the cell can be calculated by using the FOMe expression given in Eq. (26).

$$V_{cell} = E + \eta_{c_e} + \eta_{ct} + R_{ohm} \cdot I \tag{26}$$

3.2. Aging mechanisms in FOMeA

The cycle of cell charge and discharge is accompanied by the SEI layer formation and lithium plating-stripping side reactions. These side reactions lead to the loss of lithium-ions, SEI layer growth, lithium plating, and a reduction in electrolyte volume. There is a little of loss of the electrode active material with the cell aging, and the amount of loss of active material is difficult to obtain. Therefore, the changes in the amount of active material in FOMeA are ignored. The total amount of loss of lithium-ions can be calculated by summing the integration of j_{SEI}, j_{LP}, j_{LS}, and $j_{SEI,sec}$ over the thickness of negative electrode

$$\begin{aligned}\frac{\partial q_{LLI}}{\partial t} &= \frac{\partial q_{SEI}}{\partial t} + \frac{\partial q_{LP}}{\partial t} - \frac{\partial q_{LS}}{\partial t} + \frac{\partial q_{SEI,\text{sec}}}{\partial t} \\ &= A\int_0^{L_n} j_{SEI} + j_{LP} + j_{LS} + j_{SEI,sec}\,dx\end{aligned} \tag{27}$$

where q_{SEI}, q_{LP}, q_{LS}, and $q_{SEI,sec}$ are the amounts of consumed lithium-ions due to SEI layer formation, lithium plating, lithium stripping, and secondary SEI layer formation reaction, respectively.

The thickness of SEI layer L_{SEI} is related to the total amount of SEI, which can be calculated by the reaction rate of the SEI layer and secondary SEI layer formation, as shown in Eq. (28).

$$\frac{\partial L_{SEI}}{\partial t} = \frac{M_{SEI}}{n_{SEI}F\rho_{SEI}} \cdot j_{SEI} + \frac{M_{SEI}}{n_{SEI}F\rho_{SEI}} \cdot j_{SEI,\text{sec}} \tag{28}$$

where M_{SEI} is the molar mass of the SEI, ρ_{SEI} is the density of SEI. One mol SEI layer consumes two mol lithium-ions, so the value of the coefficient n_{SEI} is 2. As the cell ages, the resistance of SEI can be calculated as

$$R_{SEI} = \frac{L_{SEI}}{\kappa_{SEI}} \tag{29}$$

where κ_{SEI} is the conductivity of the SEI layer.

The thickness of plated dead lithium L_{Li} is related to the reaction rate of lithium plating and stripping, which can be calculated as

$$\frac{\partial L_{Li}}{\partial t} = \frac{M_{Li}}{n_{LP}F\rho_{Li}}(j_{LP} - j_{LS}) \tag{30}$$

where M_{Li} is the molar mass of lithium, ρ_{Li} is the density of lithium, and the value of the coefficient n_{LP} is equal to 1. As the cell ages, the resistance of the plated dead lithium can be expressed as

$$R_{Li} = \frac{L_{Li}}{\kappa_{Li}} \tag{31}$$

where κ_{Li} is the conductivity of the plated dead lithium.

The SEI layer formation also consumes the electrolyte solvents, which reduces the electrolyte phase volume fraction ε_e of the cell. As the cell ages, the change in the electrolyte phase volume fraction can be expressed as

$$\frac{\partial \varepsilon_e}{\partial t} = \frac{j_{SEI} + j_{SEI,sec}}{FAL_{sep}\varepsilon_e^0 c_{e,0}} \tag{32}$$

where ε_e^0 is the initial electrolyte phase volume fraction, and $c_{e,0}$ is the initial electrolyte phase lithium-ions concentration.

3.3. State of health evaluation indicator

As the cell ages, the loss of lithium-ions increases, the electrolyte volume fraction decreases, and the cell resistance increases. These aging characteristics affect the performance of the cell, leading to capacity fade. Therefore, cell capacity fade is an important indicator to evaluate the SOH of the cell [33]. The SOH of the cell is defined as the rate of the present cell capacity to the new cell capacity, as shown in Eq. (33).

$$SOH = \frac{Q_{aged}}{Q_{new}} \times 100\% \tag{33}$$

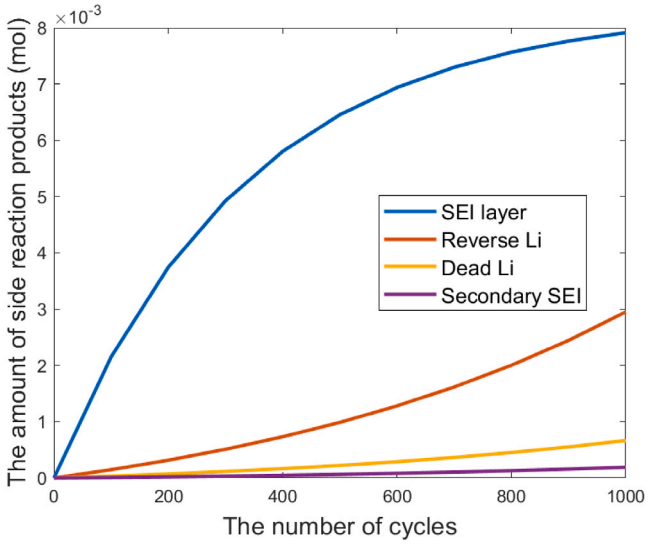

Fig. 2. The amount of side reaction products changes with the cycle number.

where Q_{aged} and Q_{new} are the capacities of the aged cell and the new cell, respectively.

The cell capacity Q_{cell} is defined as the total energy released by the cell discharges from 4.2 V (fully charged) to 2.8 V (fully discharged) at 1C rate constant current. Therefore, the cell capacity Q_{cell} can be calculated as

$$Q_{cell} = \int_0^{t_k} I(t)dt \tag{34}$$

4. Simulation and validation

A 17 Ah LMO cell is used for simulation, and the cell parameters are shown in Table 1. The cell operated with a cycling of 2C constant-current–constant-voltage (CC–CV) charge and 2C constant-current (CC) discharge at 298.15 K. The cell is cycled 1000 times and is paused every 100 cycles to obtain its internal state.

The total amount of side reaction products increases with the number of cycles, as shown in Fig. 2. All the side reaction products increase with the number of cycles. The generated SEI layer covers the negative particles, preventing further SEI layer formation side reaction. Therefore, the growth rate of the SEI layer decelerates with the increase in the number of cycles. Minimal lithium plating is observed in the first few cycles. The lithium plating overpotential η_{Li} decreases with the increase in plated lithium. Hence, the lithium plating reaction rate increases with the number of cycles. The products of lithium plating reaction are reverse lithium, dead lithium, and secondary SEI. Reverse lithium will strip into the electrolyte when $\eta_{Li} > 0$, which will not lead to lithium ion loss. Dead lithium is covered with a secondary SEI layer and cannot strip into the electrolyte. The mixture of dead lithium and secondary SEI is defined as the deposit layer.

In Fig. 3, the cell ohmic resistance increases with the increase in cycle number, and the increment of the cell resistance is mainly affected by the SEI layer resistance. Considering that the amount of the deposit layer is less than the amount of the SEI layer, and the dead lithium conductivity is relatively high, the deposit layer resistance is less than the SEI layer resistance.

The side reaction consumes the electrolyte solution, leading to a decrease in the electrolyte phase volume fraction. The changes in the electrolyte phase volume fraction with the cycle number are shown in Fig. 4.

The continuous consumption of electrolyte during cycling causes a decrease in the electrolyte phase volume fraction. However, the rate of

Table 1
The parameters of LMO battery [34].

Parameters	Negative electrode	Separator	Positive electrode
L (m)	100e−6	52e−6	183e−6
R_s (m)	12.5e−6	–	8e−6
ϵ_s	0.471	–	0.297
ϵ_e	0.4	0.4	0.4
c_s^{max} (mol/m^3)	26 390	–	22 860
c_s^0 (m^2/s)	14 870	–	3900
D_s (mol/m^3)	3.9e−14	–	1e−13
i_0 (A/m^2)	17.71	–	16.74
D_e (m^2/s)		7.5e−11	
$c_{e,0}$ (mol/m^3)		2000	
t_+		0.363	
T (K)		298.15	
F (C/mol)		96 485.33	
R_g (J/mol/K)		8.314	
R_{ohm} (Ω)		0.006	
A (m^2)		1	
κ_{SEI} (S/m)		5e−6 [35]	
M_{SEI} (kg/mol)		0.16 [35]	
ρ_{SEI} (kg/m^3)		1600 [35]	
M_{Li} (kg/mol)		6.94e−3 [12]	
ρ_{Li} (kg/m^3)		534 [12]	
j_{SEI} (A/m^2)		$6.991\times10^{-5}\times\exp(-0.2962n)$ [assumed]	
j_{Li} (A/m^2)		$3.951\times10^{-6}\times\exp(-0.1382n)$ [assumed]	
$U_p(\theta)$	$4.19829+0.0565661\tanh(-14.5546\theta+8.60942)$ $-0.0275479\left[\frac{1}{(0.998432-\theta)^{0.492465}}-1.90111\right]$ $-0.157123\exp(-0.04738\theta^8)+0.810239\exp[-40(\theta-0.133875)]$		
$U_n(\theta)$	$-0.16+1.32\exp(-3.1\theta)+10.0\exp(2000.0\theta)$		

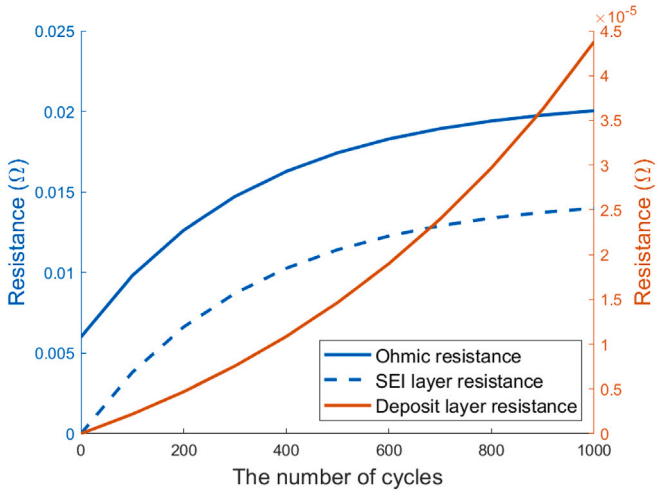

Fig. 3. Resistances comparison among the cell, SEI layer, and deposit layer with cycling.

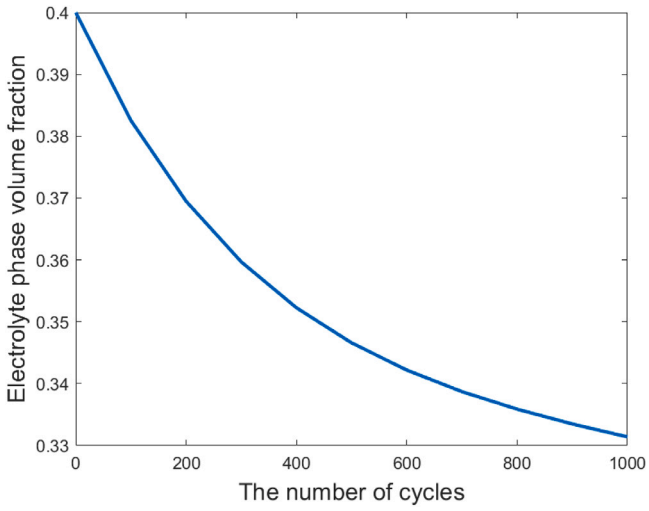

Fig. 4. The electrolyte phase volume fraction changes with cycle number.

decrease gradually decelerates because the SEI layer formation reaction also decelerates with an increase in cycle number. The decrease in electrolyte phase volume fraction affects the distribution of lithium-ions in the electrolyte. In accordance with the changes in electrolyte phase volume fraction shown in Fig. 4, the positive and negative electrolyte phase lithium-ions concentrations are calculated during 1C rate discharging and are shown in Fig. 5. The concentration of lithium-ions in the positive electrolyte increases, whereas the concentration of lithium-ions in the negative electrolyte phase decreases with the increase in cycle number. The difference between the positive and negative electrolyte phase lithium-ions concentration grows with the increase in cycle number, which increases the polarization in the electrolyte.

The loss of lithium-ions affects the initial solid phase lithium stoichiometry of the cell. The decrease in the electrolyte phase volume fraction and the increase in ohmic resistance lead to an increase in electrolyte polarization and ohmic polarization, causing the cell to reach the minimum cut-off voltage in advance during discharging. Therefore, the shift window of the solid phase surface stoichiometry narrows down with the increase in cycle number. The solid phase surface stoichiometry changes of a new cell and an aged cell under 1C rate current discharge are compared in Fig. 6. The shift window of the aged cell, which has been cycled 1000 times, is narrower than that of the new cell. The initial solid phase lithium stoichiometry of the positive and negative electrode declines slightly because the loss of lithium-ions accounts for a small part of the total lithium-ion amount of the cell.

The simulation cell is cycled 1000 times, and the comparisons of 1C constant current discharge voltage between FOMeA and P2D aging model for every 100 cycle are shown in Fig. 7. The lighter the line colo is, the higher the number of cycles is. In Fig. 7, the voltage curve of FOMeA matches the voltage curve of the P2D aging model well in

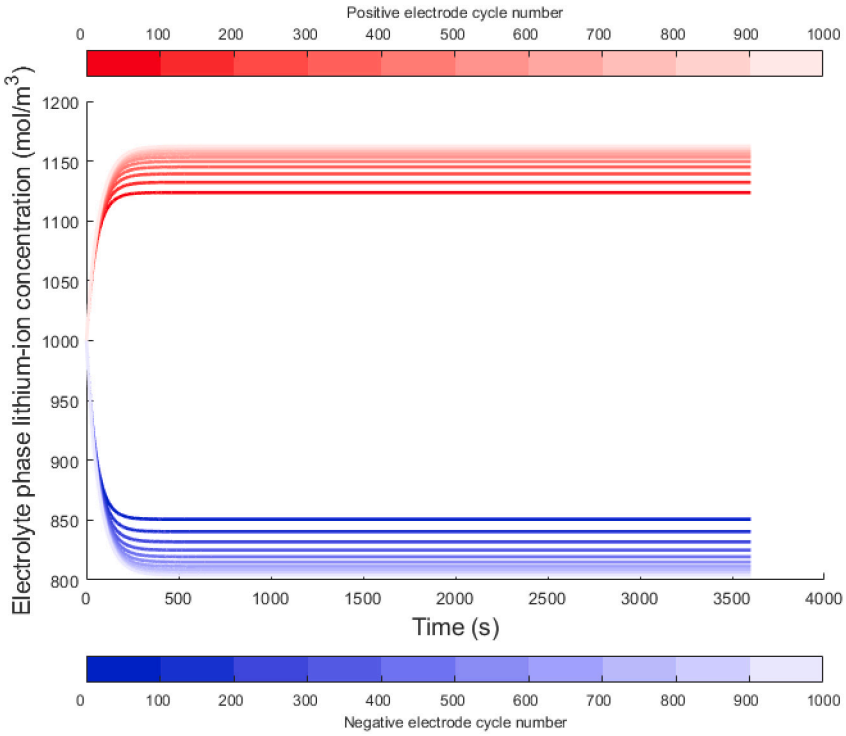

Fig. 5. The electrolyte phase lithium-ions concentrations change with cycle number.

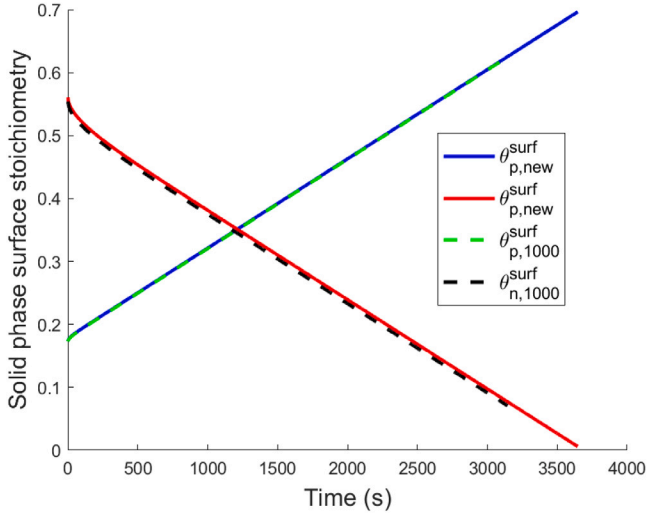

Fig. 6. The solid phase surface stoichiometry of new cell and aged cell in 1C discharging.

Table 2
Voltage RMSEs and MAPEs of FOMeA.

Cycle number	RMSE (V)	MAPE (%)
0	0.017446	0.423020
100	0.017356	0.421934
200	0.017431	0.425588
300	0.017568	0.432323
400	0.017701	0.439668
500	0.017813	0.446495
600	0.017898	0.452197
700	0.017964	0.456845
800	0.018016	0.460639
900	0.018053	0.463429
1000	0.018082	0.465546

Table 3
The computational time comparison between FOMeA and P2D aging model.

Battery aging model	Computational time
FOMeA	1.0815 s
P2D aging model	62.073 s

every cycle. The result shows that FOMeA can capture the cell aging characteristics. Even if the cell has been cycled for 1000 times, FOMeA achieves high accuracy voltage prediction. The voltage of the P2D aging model is taken as ground truth, which is compared with that of FOMeA. The root mean square error (RMSE) and the mean absolute percentage error (MAPE) between the P2D aging model and FOMeA are shown in Table 2 and Fig. 8. The maximum voltage RMSE and MAPE of FOMeA are still lower than 0.0181 V and 0.466%, respectively, although the voltage MAPE and RMSE of FOMeA increase as the number of cycles increase. Even if the cell has been cycled 1000 times, FOMeA can still achieve high-accuracy voltage prediction.

The simulations are run in Windows 11 with Intel(R) Core(TM) i7-10700F CPU @ 2.90 GHz and 32.0 GB RAM. Table 3 shows the computational time of FOMeA and the P2D aging model at 1C rate discharge with a aged cell. The simulation results show that FOMeA greatly saves computational time. The P2D aging model consumes approximately 60 times the computational time of FOMeA, making it possible to apply FOMeA to BMS for real-time SOH estimation.

The SOH comparison of the P2D aging model and FOMeA are shown in Fig. 9. The SOH of the P2D aging model is taken as the ground truth. The error between FOMeA and the P2D aging model becomes larger as the cycle number increases because of the simplification of solid and electrolyte phase lithium-ions distributions and the polarization increase in the aged cell. However, the SOH estimation error between FOMeA and the P2D aging model is only 0.86% even after 1000 cycles. The RMSE and MAPE of FOMeA for estimating SOH in a total of 1000 cycles are only 0.0065% and 0.6493%, respectively. These results indicate that FOMeA can capture the aging mechanism characteristics of lithium-ion batteries and achieve accurate estimation of SOH.

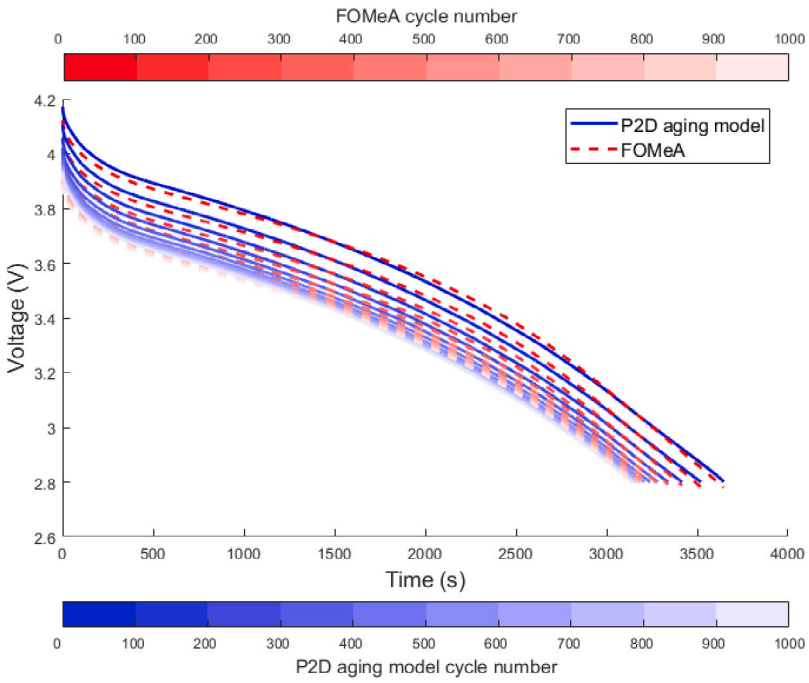

Fig. 7. 1C rate discharge voltage comparison between FOMeA and P2D aging model. (For interpretation of the references to color in this figure legend, the reader is referred to the web version of this article.)

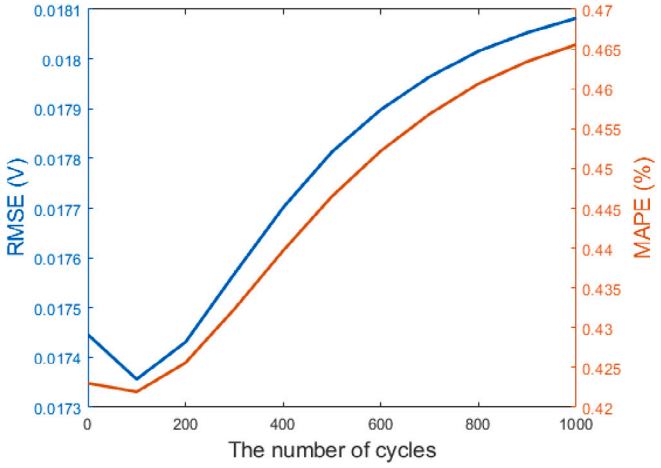

Fig. 8. Voltage RMSEs and MAPEs of FOMeA.

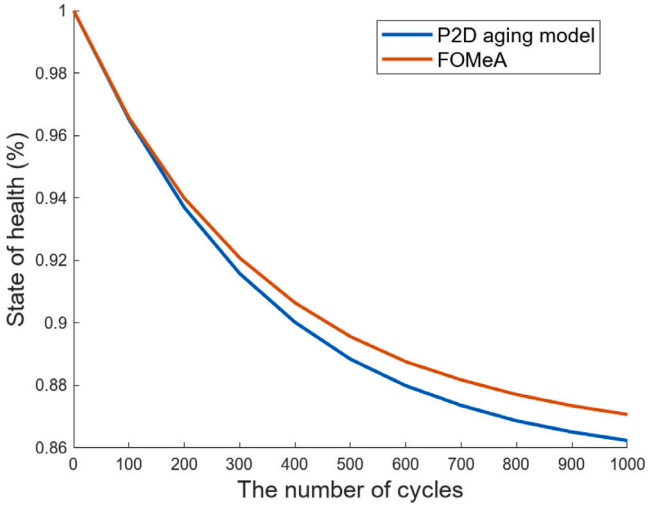

Fig. 9. SOH estimation of P2D aging model and FOMeA.

5. Conclusion

This paper proposes a FOMeA to achieve accurate SOH estimation from the perspective of aging mechanism. As the cell ages, two side reactions degrade the cell. One is the SEI layer formation side reaction that consumes electrolyte solvents and lithium-ions, leading to the loss of lithium-ions, decrease in electrolyte fractional volume, and increase in internal resistance. The other is lithium plating-stripping side reaction which consumes lithium-ion in the electrolyte. Some of the plated lithium gets covered with the secondary SEI layer, whereas others strip into the electrolyte. Therefore, the deposit layer formation leads to the loss of lithium-ions, decrease in electrolyte fractional volume, and increase in internal resistance. The electrochemical model must be simplified to apply it for SOH estimation in BMS. Hence, FOMe is proposed, which simplifies the solid phase lithium-ion distribution with the fractional-order Pade approximation method, and streamlines electrolyte phase lithium-ion distribution with a two-state system. FOMeA is built by considering the aging mechanism based on FOMe. The simulation results show that FOMeA can achieve accurate voltage prediction and SOH estimation with less computational complexity.

CRediT authorship contribution statement

Guorong Zhu: Resources, Data curation, Writing – review & editing, Funding acquisition. **Chun Kong:** Conceptualization, Methodology, Software, Validation, Writing – original draft. **Jing V. Wang:** Writing – review & editing, Investigation. **Jianqiang Kang:** Writing – review & editing, Funding acquisition, Investigation. **Qian Wang:** Writing – review & editing, Investigation. **Chunhu Qian:** Writing – review & editing, Investigation.

Declaration of competing interest

The authors declare that they have no known competing financial interests or personal relationships that could have appeared to influence the work reported in this paper.

Data availability

Data will be made available on request.

Acknowledgments

This work was supported by the National Natural Science Foundation of China under Grants No. 52277224, No. 51977163, and the foundation of Hubei province, China under Grants No 2021BAE130.

References

[1] G. Zhu, C. Kong, J.V. Wang, J. Kang, G. Yang, Q. Wang, A fractional-order model of lithium-ion battery considering polarization in electrolyte and thermal effect, Electrochim. Acta 438 (2023) 141461.
[2] H. Feng, H. Yan, State of health estimation of large-cycle lithium-ion batteries based on error compensation of autoregressive model, J. Energy Storage 52 (2022) 104869.
[3] S. Sharma, A.K. Panwar, M.M. Tripathi, Storage technologies for electric vehicles, J. Traffic Transp. Eng. 7 (3) (2020) 340–361.
[4] S. Ma, M. Jiang, P. Tao, C. Song, J. Wu, J. Wang, T. Deng, W. Shang, Temperature effect and thermal impact in lithium-ion batteries: A review, Prog. Nat. Sci.: Mater. Int. 28 (6) (2018) 653–666.
[5] D. Ren, X. Feng, L. Liu, H. Hsu, L. Lu, L. Wang, X. He, M. Ouyang, Investigating the relationship between internal short circuit and thermal runaway of lithium-ion batteries under thermal abuse condition, Energy Storage Mater. 34 (2021) 563–573.
[6] J. Li, K. Adewuyi, N. Lotfi, R.G. Landers, J. Park, A single particle model with chemical/mechanical degradation physics for lithium ion battery State of Health (SOH) estimation, Appl. Energy 212 (2018) 1178–1190.
[7] J. Vetter, P. Novák, M.R. Wagner, C. Veit, K.C. Möller, J.O. Besenhard, M. Winter, M. Wohlfahrt-Mehrens, C. Vogler, A. Hammouche, Ageing mechanisms in lithium-ion batteries, J. Power Sources 147 (1) (2005) 269–281.
[8] S. Phul, A. Deshpande, B. Krishnamurthy, A Mathematical model to study the effect of potential drop across the SEI layer on the capacity fading of a lithium ion battery, Electrochim. Acta 164 (2015) 281–287.
[9] A. Wang, S. Kadam, H. Li, S. Shi, Y. Qi, Review on modeling of the anode solid electrolyte interphase (SEI) for lithium-ion batteries, npj Comput. Mater. 4 (1) (2018) 1–26.
[10] D. Ren, X. Feng, L. Lu, X. He, M. Ouyang, Overcharge behaviors and failure mechanism of lithium-ion batteries under different test conditions, Appl. Energy 250 (2019) 323–332.
[11] B. Ghanbarzadeh, A. Khatibi, A. Asadi, B. Shokri, Regulating lithium-ion flux in the solid electrolyte interphase layer to prevent lithium dendrite growth on lithium metal anode, J. Energy Storage 47 (2022) 103668.
[12] D. Ren, K. Smith, D. Guo, X. Han, X. Feng, L. Lu, M. Ouyang, J. Li, Investigation of lithium plating-stripping process in Li-ion batteries at low temperature using an electrochemical model, J. Electrochem. Soc. 165 (10) (2018) A2167.
[13] Y. Yang, L. Xu, S.-J. Yang, C. Yan, J.-Q. Huang, Electrolyte inhomogeneity induced lithium plating in fast charging lithium-ion batteries, J. Energy Chem. 73 (2022) 394–399.
[14] X. Han, X. Feng, M. Ouyang, L. Lu, J. Li, Y. Zheng, Z. Li, A comparative study of charging voltage curve analysis and state of health estimation of lithium-ion batteries in electric vehicle, Automot. Innov. 2 (4) (2019) 263–275.
[15] X. Han, M. Ouyang, L. Lu, J. Li, Y. Zheng, Z. Li, A comparative study of commercial lithium ion battery cycle life in electrical vehicle: Aging mechanism identification, J. Power Sources 251 (2014) 38–54.
[16] J. Tian, R. Xiong, Q. Yu, Fractional-order model-based incremental capacity analysis for degradation state recognition of lithium-ion batteries, IEEE Trans. Ind. Electron. 66 (2019) 1576–1584.
[17] Y. Bi, Y. Yin, S.-Y. Choe, Online state of health and aging parameter estimation using a physics-based life model with a particle filter, J. Power Sources 476 (2020) 228655.
[18] R. Xiong, J. Tian, W. Shen, J. Lu, F. Sun, Semi-supervised estimation of capacity degradation for lithium ion batteries with electrochemical impedance spectroscopy, J. Energy Chem. 76 (2023) 404–413.
[19] S. Shen, M. Sadoughi, M. Li, Z. Wang, C. Hu, Deep convolutional neural networks with ensemble learning and transfer learning for capacity estimation of lithium-ion batteries, Appl. Energy 260 (2020) 114296.
[20] M. Doyle, T.F. Fuller, J. Newman, Modeling of galvanostatic charge and discharge of the lithium/polymer/insertion cell, J. Electrochem. Soc. 140 (6) (1993) 1526.
[21] S. Han, Y. Tang, S. Khaleghi Rahimian, A numerically efficient method of solving the full-order pseudo-2-dimensional (P2D) Li-ion cell model, J. Power Sources 490 (2021) 229571.
[22] S. Santhanagopalan, Q. Guo, P. Ramadass, R.E. White, Review of models for predicting the cycling performance of lithium ion batteries, J. Power Sources 156 (2) (2006) 620–628.
[23] D. Guo, G. Yang, X. Feng, X. Han, L. Lu, M. Ouyang, Physics-based fractional-order model with simplified solid phase diffusion of lithium-ion battery, J. Energy Storage 30 (2020) 101404.
[24] X. Han, M. Ouyang, L. Lu, J. Li, Simplification of physics-based electrochemical model for lithium ion battery on electric vehicle. Part I: Diffusion simplification and single particle model, J. Power Sources 278 (2015) 802–813.
[25] S.J. Moura, F.B. Argomedo, R. Klein, A. Mirtabatabaei, M. Krstic, Battery state estimation for a single particle model with electrolyte dynamics, IEEE Trans. Control Syst. Technol. 25 (2) (2017) 453–468.
[26] X. Li, G. Fan, K. Pan, G. Wei, C. Zhu, G. Rizzoni, M. Canova, A physics-based fractional order model and state of energy estimation for lithium ion batteries. Part I: Model development and observability analysis, J. Power Sources 367 (2017) 187–201.
[27] X. Li, K. Pan, G. Fan, R. Lu, C. Zhu, G. Rizzoni, M. Canova, A physics-based fractional order model and state of energy estimation for lithium ion batteries. Part II: Parameter identification and state of energy estimation for LiFePO4 battery, J. Power Sources 367 (2017) 202–213.
[28] S.J. An, J. Li, C. Daniel, D. Mohanty, S. Nagpure, D.L. Wood, The state of understanding of the lithium-ion-battery graphite solid electrolyte interphase (SEI) and its relationship to formation cycling, Carbon 105 (2016) 52–76.
[29] W. Cai, C. Yan, Y.-X. Yao, L. Xu, X.-R. Chen, J.-Q. Huang, Q. Zhang, The boundary of lithium plating in graphite electrode for safe lithium-ion batteries, Angew. Chem. Int. Ed. 60 (23) (2021) 13007–13012.
[30] C. Li, N. Cui, C. Wang, C. Zhang, Simplified electrochemical lithium-ion battery model with variable solid-phase diffusion and parameter identification over wide temperature range, J. Power Sources 497 (2021) 229900.
[31] W. Luo, C. Lyu, L. Wang, L. Zhang, An approximate solution for electrolyte concentration distribution in physics-based lithium-ion cell models, Microelectron. Reliab. 53 (6) (2013) 797–804.
[32] C. Li, N. Cui, C. Wang, C. Zhang, Reduced-order electrochemical model for lithium-ion battery with domain decomposition and polynomial approximation methods, Energy 221 (2021) 119662.
[33] E. Liu, G. Niu, X. Wang, B. Zhang, SOH diagnostic and prognostic based on external health indicator of lithium-ion batteries, in: IECON 2021 – 47th Annual Conference of the IEEE Industrial Electronics Society, 2021, pp. 1–6, http://dx.doi.org/10.1109/IECON48115.2021.9589170.
[34] M. Doyle, J. Newman, A.S. Gozdz, C.N. Schmutz, J.-M. Tarascon, Comparison of modeling predictions with experimental data from plastic lithium ion cells, J. Electrochem. Soc. 143 (6) (1996) 1890.
[35] H. Ekström, G. Lindbergh, A model for predicting capacity fade due to SEI formation in a commercial graphite/LiFePO4 cell, J. Electrochem. Soc. 162 (6) (2015) A1003.